Gas-Phase Chemistry of Bare V^+ Cation with Oxygen and Water at Room Temperature: Formation and Hydration of Vanadium Oxide Cations

Gregory K. Koyanagi and Diethard K. Bohme*

Department of Chemistry, Centre for Research in Mass Spectrometry, Centre for Research in Earth and Space Science, York University, Toronto, Ontario, Canada M3J 1P3

Ilona Kretzschmar, Detlef Schröder,* and Helmut Schwarz*

Institut für Organische Chemie der Technischen Universität Berlin, Strasse des 17. Juni 135, D-10623 Berlin, Germany

Received: November 14, 2000; In Final Form: February 20, 2001

Mass spectrometric experiments at extremely low ($<10^{-6}$ mbar) and moderate (0.5 mbar) pressures are used to examine the reactions of atomic vanadium cation with molecular oxygen and water. With O_2, rapid O-atom abstraction gives rise to the formation of VO^+ cation ($k = 3 \times 10^{-10}$ cm^3 molecule^{-1} s^{-1}). Interestingly, despite a similar thermochemistry, the O-atom transfer from water to bare V^+ is less efficient by more than an order of magnitude ($k = 8 \times 10^{-12}$ cm^3 molecule^{-1} s^{-1}). Subsequent associations of VO^+ with either O_2 or H_2O occur with very low efficiencies and involve termolecular stabilization mechanisms. The low probability of degenerate $^{16}O/^{18}O$ exchange between VO^+ and water indicates the operation of a sizable kinetic barrier. Ab initio calculations using density functional theory lend further support to the interpretation of the experimental data and provide the first thermochemical information on VO_n^+ cations with $n > 2$, as well as some hydrated species. In general, the dipolar water ligand is found to be much more strongly bound to the cationic vanadium complexes than is dioxygen.

Introduction

Vanadium oxides are among the most important transition-metal catalysts applied in chemical technology.[1] Their uses range from the production of sulfuric acid, via selective oxidations of aliphatic and aromatic hydrocarbons, to epoxidation catalysis. As an early transition metal, vanadium is very oxophilic and thus is likely to exist in its higher valency states in the presence of oxidizing agents. In turn, high-valent vanadium compounds are required at the catalytically active sites relevant in oxygenation processes. Further, in an excess of oxidant, peroxidic structures may be accessed. Previous matrix isolation studies[2] and anion photodetachment spectroscopy[3] have provided evidence for the existence of vanadium peroxides, such as $O_2V(O_2)$, in idealized environments. In the condensed phase, ligated vanadium peroxides ($L_mV(O_2)_n$; $n = 1-4$) have wide applications ranging from synthetic interests to the treatment of diabetics.[4]

The present study describes the chemistry initiated by V^+ in O_2 at room temperature and the formation of the higher oxides $[V,O_n]^+$ with $n \leq 7$. To this end, Fourier transform mass spectrometry and selected-ion flow tube techniques are combined with a theoretical investigation of gaseous $[V,O_n]^+$ cations by means of density functional theory. Reactions of vanadium containing cations with water, inter alia leading to formally hydrated oxide ions, such as the $OV(OH_2)^+/V(OH)_2^+$ couple, also are examined.

Experimental Methods

The formation of vanadium oxide ions is achieved in reactions initiated by atomic V^+ cations in the presence of molecular oxygen. These reactions are investigated with both the Fourier transform ion-cyclotron resonance (FTICR) instrument at the Technical University in Berlin and the inductively-coupled plasma/selected-ion flow tube mass spectrometer (ICP/SIFT) instrument in the Ion-Chemistry Laboratory at York University.

FTICR. These experiments use a Spectrospin CMS 47X FTICR mass spectrometer equipped with an external ion source as described elsewhere.[5,6] In brief, V^+ is generated by laser ablation of a vanadium target using a Nd:YAG laser operating at 1064 nm. A series of potentials and ion lenses is used to transfer the ions to the ICR cell, which is positioned in the bore of a 7.05 T superconducting magnet. Mass-selected $^{51}V^+$ is then thermalized by nonreactive collisions with pulsed-in argon buffer gas, followed by reisolation of the metal ion and monitoring the reaction with molecular oxygen leaked-in at constant pressures ranging from 1 to 3×10^{-8} mbar. The experimental second-order rate constants are evaluated assuming the pseudo first-order kinetic approximation after calibration of the measured pressures and acknowledgment of the ion gauge sensitivities; the error of the absolute rate constants is ±30%, and the ion temperature is assumed to be 298 K.[7] To provide a solid basis for the analysis of consecutive reaction kinetics and for the comparison with the SIFT data, all experiments are conducted at three different pressures. The kinetic modeling applied here is based on simple rate expressions and iterative procedures for data fitting using Excel 2000.

ICP/SIFT. The SIFT instrument is described in detail elsewhere.[8] V^+ ions are generated in an inductively coupled plasma (ICP) and introduced into the SIFT through an atmosphere/vacuum interface. The ICP ion source and the interface are shown schematically in Figure 1.[9] A radio frequency power

10.1021/jp004197t CCC: $20.00
Published on Web 04/07/2001

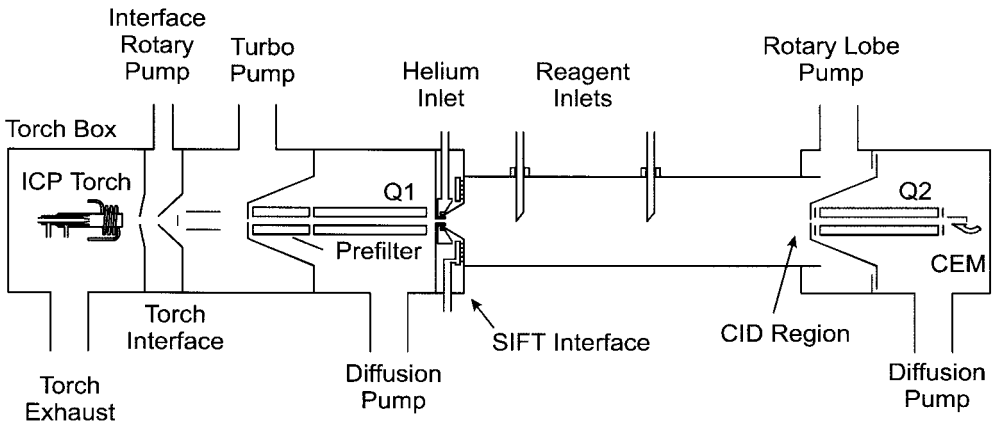

Figure 1. Schematic view of the ICP/SIFT apparatus.

supply and ICP torch assembly (standard concentric design) from a commercial instrument (ELAN series, PE/SCIEX) have been modified for stand-alone operation. Typical parameters are as follows: the rf power supply is set to transmit 1250 W of power (free-running frequency, 40 MHz), and the flows of argon into the three torch inputs are adjusted to 14 to 15 l min^{-1} (outer gas), 2 l min^{-1} (intermediate or plasma gas), and 1.2 l min^{-1} (inner or nebulizer gas). The ICP/SIFT interface consists of differentially pumped sampling and skimmer cones with orifice diameters of 1.14 and 0.88 mm, respectively, and a 5.0 mm shadow stop to block out UV photons. The region between the sampling cone and skimmer is pumped by a 1000 l min^{-1} rotary vane pump (Alcatel 2060) and the region after the skimmer is pumped by a 200 l s^{-1} turbo-molecular pump (Leybold Hy.Cone 200). The existing quadrupole for reagent ion selection has been augmented with an rf-only quadrupole prefilter 116 mm in length. This prefilter is capacitively coupled to the resolving quadrupole with a matched set of high-voltage 100 pf capacitors. Typically, the prefilters are floated at −36 V with respect to the instrument ground coupled through 20 MΩ resistors.

The vanadium salt solution is derived from a 1000 μg ml^{-1} atomic spectroscopy standard solution of ammonium metavanadate, NH_4VO_3 (PE pure grade, stabilized with 2% nitric acid), diluted 25:1 to 40 μg mL^{-1}. It is peristatically pumped (Gilson Minipuls 3, two channel) to a nebulizer at 0.6 mL min^{-1}. The nebulizer is of crossed-flow gem-tip design, spraying into a Scott-type double-pass chamber. The nebulized solution is carried to the plasma region by an alumina injector. The sampled plasma ions are filtered with a quadrupole mass filter (Q1 in Figure 1) and injected into the flow tube through a Venturi-type interface. Helium is used as the SIFT buffer gas at 0.47 mbar and a flow-tube temperature of 296 ± 2 K. The selected ions entering the flow tube are allowed to thermalize by collisions with He (ca. 4×10^5 collisions) prior to reaching the reaction region further downstream at the point of addition of the reagent gas. The extent to which thermalization of atomic vanadium cation is achieved is unknown, however, and quenching of the excited ^5F state of atomic V^+ cation by collision with rare gases appears to be particularly difficult.[10] According to known electronic states,[11] V^+ emerges in the ^5D, ^5F, ^3F, ^3P, and ^5H states with electronic energies (lowest microstate) of 0, 0.32, 1.1, 1.4, and 1.55 eV, respectively, in a population distribution of 60:29:3:1:1 at a nominal plasma temperature of 5500 K. However, the experiments reported here give no obvious indication for the presence of more than one electronic state of V^+ in the reaction region. In the reaction with O_2, the observed decay of V^+ is linear over more than two decades. Reactant and product ions are monitored still further downstream by sampling with a skimmer and analyzing the ions with a second quadrupole mass filter (Q2). Ions are counted with a channeltron electron multiplier. Further, nose-cone voltage experiments are conducted to probe the bond connectivities of some of the vanadium oxide ions by multicollision induced dissociation. The reagents O_2 (Matheson, UHP, 99.8% min) and D_2O (MSD Isotopes, 99.8 atom % D) are used as purchased; D_2O is added into the reaction region as a 3% mixture in helium. Reaction rate constants are determined from the measured semilogarithmic decay of the reactant ion as a function of the flow of the added reagent gas.

TABLE 1: Comparison of Calculated and Experimental Properties of Small Ions and Molecules (all properties in eV)

property	calcd	exptl	deviation (rel.)
D_0(O−O)	5.11	5.116 ± 0.001[a]	0.006 (0.1%)
D_0(V^+−O)	5.46	5.99 ± 0.10[b]	0.53 (8.8%)
D_0(V−O)	6.30	6.49 ± 0.09[c]	0.19 (2.9%)
IE(V)	6.57	6.74[d]	0.17 (2.5%)
IE(VO)	7.42	7.2386[e]	−0.18 (2.5%)
D_0(HO−H)	4.88	5.11 ± 0.01[a]	0.23 (4.5%)

[a] Chase, M. W., Jr.; Davies, C. A.; Downey, J. R., Jr.; Frurip, D. J.; McDonald, R. A.; Syverud, A. N. *J. Phys. Chem. Ref. Data* **1985**, *14*, Suppl. 1 (JANAF Tables). [b] Clemmer, D. E.; Aristov, N.; Armentrout, P. B. *J. Phys. Chem.* **1993**, *97*, 544. [c] Reference 21. [d] Reference 11. [e] Reference 37.

Theoretical Methods

The geometries and energetics of the vanadium oxide species reported here are obtained at the density functional level of theory using the Becke3LYP hybrid method[12] as implemented in the Gaussian94 program package[13] in combination with triple-ζ quality valence basis sets (TZV) for oxygen and vanadium as developed by Ahlrichs.[14] The oxygen and vanadium basis sets are complemented with an additional p and d polarization function,[15] respectively. The comparable valence triple-ζ basis from Ahlrichs, also complemented with an additional polarization function, is used for hydrogen.[15]

To determine the suitability of these basis sets for the problems tackled here, some test calculations have been performed. As can be seen from the data summarized in Table 1, the bond dissociation and ionization energies of small fragments such as V, VO, O_2, and H_2O are properly described within ca. 5% of the experimental values. The large deviation of 8.8% for D_0(V^+−O) can be attributed to the inappropriate description of the bare vanadium cation with the B3LYP approach; for a detailed discussion, see ref 16. All stationary points are fully optimized geometries and characterized as minima or first-order transition structures by frequency calcula-

tions. In cases where transition structures are reported, their connection to minima is assured by internal reaction coordinate (IRC) calculations. All energies reported include corrections for zero-point vibrational energy (ZPVE), unless stated otherwise. The computations have been performed on either IBM/RS 6000 workstations or a CRAY−YMP supercomputer.

Experimental Results

The mass-spectrometric experiments use two complementary techniques. FTICR ensures strictly bimolecular reactions due to the extremely low-pressure regime applied ($<10^{-6}$ mbar). Accurate precursor ion selection and high mass resolution allow for a safe assignment of the ions observed to specific chemical processes. In turn, the SIFT experiments involve typical operating pressures in the mbar regime, thereby ensuring effective ion thermalization and allowing for association reactions via termolecular stabilization with the helium buffer gas. As demonstrated previously, the two methods can complement each other and lead to internally consistent results.[7]

FTICR Experiments. Under low pressure conditions of FTICR experiments, the only process observed when trapping vanadium cation in molecular oxygen is oxygen atom transfer according to reaction 1.

$$V^+ + O_2 \rightarrow VO^+ + O \qquad (1)$$

The average of the experimental rate constants determined at three different pressures amounts to $(2.67 \pm 0.22) \times 10^{-10}$ cm^3 molecule^{-1} s^{-1}; consideration of the error in the absolute pressure measurement leads to $k_1 = (2.7 \pm 0.8) \times 10^{-10}$ cm^3 molecule^{-1} s^{-1} as a conservative estimate. This value corresponds to a reaction efficiency of 40% relative to the gas-kinetic collision rate[17] of 6.6×10^{-10} cm^3 molecule^{-1} s^{-1}. A previous ICR study of reaction 1 gave a rate constant about twice as high as our value.[18] However, we prefer our result as these authors similarly overestimated the rate constant for the Fe^+/N_2O system,[19] which has been analyzed more recently in some detail.[7,20] Aside from the excellent agreement with the SIFT data reported below, preference for our value of k_1 is further supported by guided ion beam studies of Armentrout and coworkers[21] in which an efficiency of 50% was reported for reaction 1. At longer reaction times, other products are formed in small amounts, such as VOH_n^+ ($n = 1, 2$) and $VO_2H_n^+$ ($n = 0-2$), which are due to background contaminants present in the high-vacuum system, inter alia water, and show characteristic day-to-day variations.

If water is deliberately added, bare V^+ reacts almost exclusively under formation of VO^+ according to reaction 2a.[22] Interestingly, the formal adduct ion $[V,O,H_2]^+$ is also observed in low but yet significant abundances (reaction 2b, branching ratio ca. 1%).[23]

$$V^+ + H_2O \rightarrow VO^+ + H_2 \qquad (2a)$$

$$\rightarrow [V,O,H_2]^+ \qquad (2b)$$

Despite being considerably exothermic (0.95 eV at 0 K), reaction 2 proceeds rather slowly with $k_2 = (8.3 \pm 2.5) \times 10^{-12}$ cm^3 molecule^{-1} s^{-1} which corresponds to less than one percent of the gas kinetic collision rate of 2.6×10^{-9} cm^3 molecule^{-1} s^{-1}. Qualitatively, this result is consistent with reaction 2a being kinetically controlled as predicted by Irigoras et al.[16] Quantitatively, however, their computed barrier height of 0.6 eV above the entrance channel seems to be slightly too large for the reaction to occur at any notable extent at room temperature.

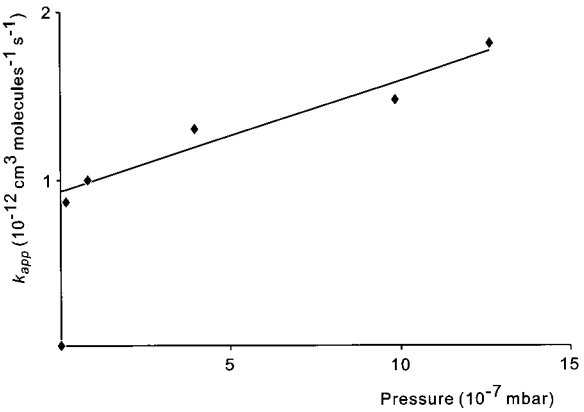

Figure 2. Apparent rate constant for association of VO^+ with water as a function of water pressure as determined by FTICR measurements.

Subsequently, the VO^+ ion undergoes clustering with water according to reaction 3 to yield $[V,O_2,H_2]^+$. Kinetic analysis implies that the minor $[V,O,H_2]^+$ product also affords the $[V,O_2,H_2]^+$ ion in the presence of water concomitant with loss of molecular hydrogen (reaction 4).

$$VO^+ + H_2O \rightarrow [V,O_2,H_2]^+ \qquad (3)$$

$$[V,O,H_2]^+ + H_2O \rightarrow [V,O_2,H_2]^+ + H_2 \qquad (4)$$

Ligand association in the highly diluted gas phase is likely to involve radiative as well as termolecular processes.[24] Not at all unexpected for such a small system, the association reaction 3 is inefficient in the pressure regime of the ICR experiments.[25] Examination of reaction 3 at different water pressures allows the deconvolution of the radiative and termolecular contributions to the apparent bimolecular rate constant $k_{3,app}$.

The data shown in Figure 2 lead to the expression $k_{3,app} = (9 \pm 3) \times 10^{-12}$ cm^3 molecule^{-1} s^{-1} + $(2.5 \pm 1.5) \times 10^{-23}$ cm^6 molecules^{-2} s^{-1} $\times$ $p(H_2O)$; here, the first term expresses the radiative stabilization of the transient $[V,O_2,H_2]^+$ species and the second term represents termolecular stabilization with water acting as a third body. Subsequently, the $[V,O_2,H_2]^+$ product continues clustering with water, reactions 5 and 6.

$$[V,O_2,H_2]^+ + H_2O \rightarrow [V,O_3,H_4]^+ \qquad (5)$$

$$[V,O_3,H_4]^+ + n\,H_2O \rightarrow [V,O_{3+n},H_{4+2n}]^+ \qquad (6)$$

Not surprisingly, the apparent rates of association increase with the number of water ligands, for example, k_5 is about four times larger than k_3. However, in view of the increasing complexity of the underlying kinetic schemes and evident signals due to background contaminants, we refrain from further analysis of the subsequent association kinetics of these experiments.

$$V^{18}O^+ + H_2{}^{16}O \rightarrow V^{16}O^+ + H_2{}^{18}O \qquad (7)$$

Although it is somewhat confusing at first glance, $^{16}O/^{18}O$-isotopic labeling turns out to be most instructive. In the reaction of water with mass-selected $V^{18}O^+$, generated according to reaction 1 using $^{18}O_2$, degenerate isotope exchange is observed according to reaction 7. However, the rate constant $k_7 = (5 \pm 2) \times 10^{-13}$ cm^3 molecule^{-1} s^{-1} is surprisingly small compared to half of the collision rate (2.5×10^{-9} cm^3 molecule^{-1} s^{-1}) expected for a thermoneutral isotope exchange. In fact, isotope

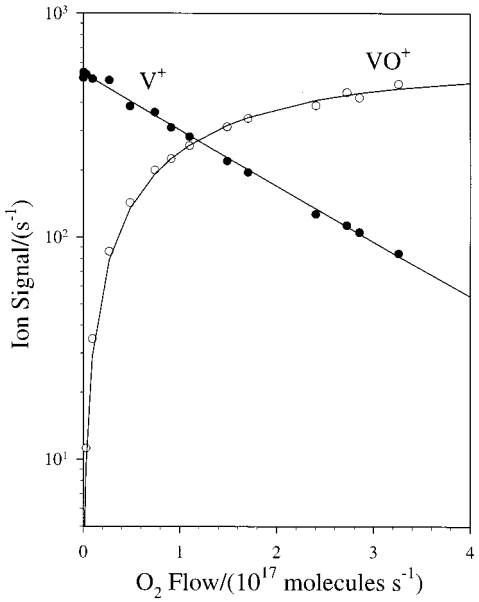

Figure 3. Reaction profile obtained with the ICP/SIFT apparatus for the oxidation reaction of V^+ with O_2 at low additions of oxygen.

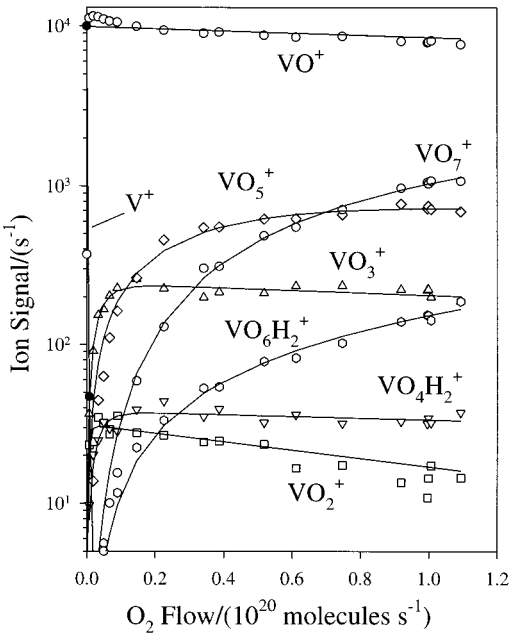

Figure 4. Reaction profiles obtained with the ICP/SIFT apparatus for the higher order oxidation chemistry initiated by V^+ in O_2 at high additions of oxygen.

exchange and association of a water ligand effectively compete with each other, even in the low pressure regime of ICR experiments. This observation suggests that the initially formed encounter complex $^{18}OV(^{16}OH_2)^+$ can barely interconvert to the quasi-symmetric dihydroxide ion $(H^{18}O)V(^{16}OH)^+$, which may serve as an intermediate in $^{16}O/^{18}O$ exchange. Vanadium is quite different from the few other transition metals studied in this particular respect. For example, though not occurring at collision rate, $^{16}O/^{18}O$ exchanges are only moderately kinetically hindered in the systems FeO^+/H_2O,[26] $FeOH^+/H_2O$,[26,27] $Fe_2O_2^+/H_2O$,[28] and PtO_2^+/H_2O.[29] Moreover, VO_2^+ undergoes efficient $^{16}O/^{18}O$ exchange in the presence of water.[30]

Interestingly, the $[V,^{16}O,^{18}O,H_2]^+$ species formed by the association of $V^{18}O^+$ with (unlabeled) water in analogy to reaction 3 undergoes much more rapid depletion of the ^{18}O label in the presence of water, reaction 8; note that for this degenerate isotope exchange, the maximum is one third of the collision rate on statistical grounds.

$$[V,^{16}O,^{18}O,H_2]^+ + H_2{}^{16}O \rightarrow [V,O_2,H_2]^+ + H_2{}^{18}O \quad (8)$$

Kinetic modeling of the time dependencies of the various ion intensities gives $k_8 = (5 \pm 3) \times 10^{-11}$ cm^3 molecule^{-1} s^{-1}, i.e., ca. 100 times faster $^{16}O/^{18}O$ exchange than in reaction 7. Qualitatively, this result suggest that the oxygen atoms in $[V,^{16}O,^{18}O,H_2]^+$ are equilibrated, thus implying facile interconversion of $OV(OH_2)^+$ and $V(OH)_2^+$ for the long-lived ion. This is precisely the opposite of the above deduction. As outlined in the discussion, these seemingly contradictory results are in fact quite instructive as far as energetic and structural aspects of the $[V,O_2,H_2]^+$ system are concerned.

ICP/SIFT Experiments. The results of the reaction of V^+ with oxygen using the ICP/SIFT apparatus are shown in Figures 3 and 4. V^+ is observed to react rapidly with oxygen by oxygen atom transfer according to reaction 1 with $k_1 = 2.8 \times 10^{-10}$ cm^3 molecule^{-1} s^{-1}; for all SIFT experiments, the error of the absolute rate constants amounts to 30%.

In addition, a small amount of the vanadium dioxide cation VO_2^+ is detected under SIFT conditions. The minor VO_2^+ channel in Figure 4 can be attributed to the occurrence of some association according to reaction 9 with an approximate branching ratio k_9/k_1 of 0.003. The formation of the association complex is presumed to occur by collisional stabilization of the encounter complex with helium.

$$V^+ + O_2 \rightarrow VO_2^+ \quad (9)$$

Higher-order reactions are observed at larger flows of O_2. Thus, VO^+ continues to react with oxygen in reaction 10, but only very sluggishly, with an effective bimolecular rate coefficient of $k_{10} = 2.0 \times 10^{-13}$ cm^3 molecule^{-1} s^{-1} under SIFT conditions.

$$VO^+ + O_2 \rightarrow [V,O_3]^+ \quad (10)$$

Despite the weakness of the $[V,O_3]^+$ signal, oxygen addition according to reaction 10 appears as the main reaction channel of VO^+. This first association step is followed by rapid additions of two further oxygen molecules according to reactions 11 and 12.

$$[V,O_3]^+ + O_2 \rightarrow [V,O_5]^+ \quad (11)$$

$$[V,O_5]^+ + O_2 \rightarrow [V,O_7]^+ \quad (12)$$

Kinetic fits of the $[V,O_n]^+$ ion profiles provide rate coefficients of $k_{11} = 7.3 \times 10^{-12}$ and $k_{12} = 2.0 \times 10^{-12}$ cm^3 molecule^{-1} s^{-1}, respectively. Reactions 9 to 12 are presumed to occur by termolecular association, with helium (and oxygen) acting as the stabilizing third body. There is no evidence for the addition of a fourth oxygen molecule to form $[V,O_9]^+$; the kinetic fit in Figure 4 provides an upper limit of $\leq 3 \times 10^{-13}$ cm^3 molecule^{-1} s^{-1} for further reactions of $[V,O_7]^+$. Multicollision induced dissociation experiments in He buffer indicate sequential losses of three O_2 molecules from $[V,O_7]^+$, i.e., the reverse of reactions 10−12.

Similar to the ICR experiments, the reaction of V^+ with D_2O was investigated independently. The deuterated analogues of both channels 2a and 2b were observed with $k_2 = 1.0 \times 10^{-11}$ cm^3 molecule^{-1} s^{-1} and a branching ratio for channel 2b of 2 ± 1%. These results are consistent with the ICR measurements

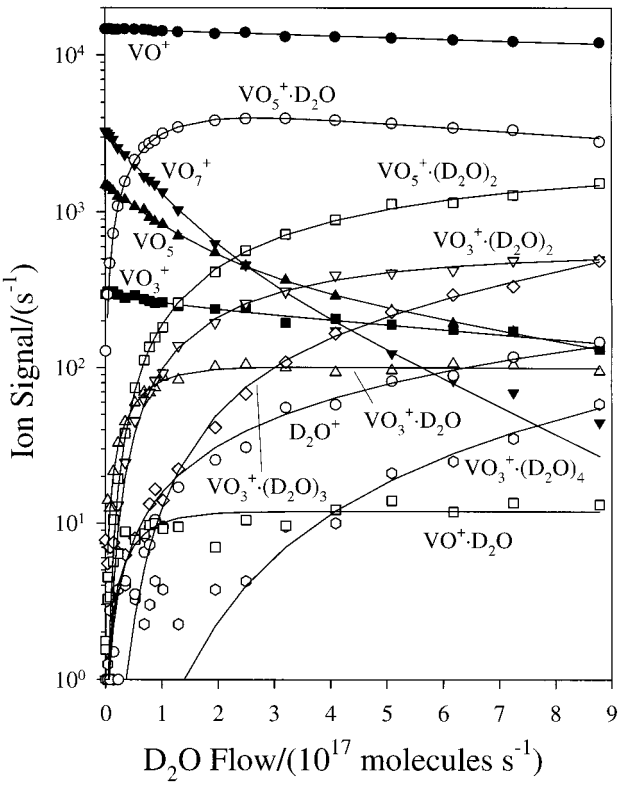

Figure 5. Reaction profiles obtained with the ICP/SIFT apparatus for reactions of $[V,O_n]^+$ ions with D_2O at an O_2 flow of 1.0×10^{20} molecules s^{-1} added upstream in the flow tube.

and suggest that helium is not very effective in the collisional stabilization of the adduct ion at 0.35 Torr.

The appearance of $[V,O_4,H_2]^+$ and $[V,O_6,H_2]^+$ in Figure 4 is attributed to the presence of water as a contaminant in the flow system. To further elucidate these hydration processes, O_2 is added upstream at a sufficient flow (ca. 10^{20} molecules s^{-1}) to establish the higher $[V,O_n]^+$ ions, whereas D_2O is deliberately added further downstream (Figure 5). The water chemistry appears to be dominated by the exchange reactions of $[V,O_5]^+$ and $[V,O_7]^+$ with water, reactions 13 and 14, followed by subsequent hydrations with further water molecules.

$$[V,O_5]^+ + D_2O \rightarrow [V,O_4,D_2]^+ + O_2 \qquad (13)$$

$$[V,O_7]^+ + D_2O \rightarrow [V,O_6,D_2]^+ + O_2 \qquad (14)$$

The ions formed can be regarded formally as hydrated vanadium oxide ions, i.e., $[V,O_3]^+\bullet(D_2O)_n$ and $[V,O_5]^+\bullet(D_2O)_n$, respectively, and are observed with n up to 6. According to the initial slopes of the decays of $[V,O_5]^+$ and $[V,O_7]^+$ shown in Figure 5, lower estimates for the rate coefficients of reactions 13 and 14 can be derived as $\geq 3.2 \times 10^{-10}$ and $\geq 5.0 \times 10^{-10}$ cm^3 $molecule^{-1}$ s^{-1}, respectively. Instead, VO^+ appears to react only slowly with D_2O according to reaction 15, with an apparent rate constant of 1.3×10^{-11} cm^3 $molecule^{-1}$ s^{-1}.

$$VO^+ + D_2O \rightarrow [V,O_2,D_2]^+ \qquad (15)$$

Only small amounts of $[V,O_2,D_2]^+$ are formed at high flows of D_2O, as would be expected if this ion reacts further with D_2O and/or O_2 (see below). Therefore, only a lower limit $\geq 4.8 \bullet \times 10^{-11}$ cm^3 $molecule^{-1}$ s^{-1} can be assigned to the reaction of $[V,O_3]^+$ with D_2O because both the association reaction (16a) and the ligand-exchange process (16b) are feasible channels, and the presence of high amounts of O_2 in the flow may drive reaction 16b also in the reverse direction.

$$[V,O_3]^+ + D_2O \rightarrow [V,O_4,D_2]^+ \qquad (16a)$$

$$\rightarrow [V,O_2,D_2]^+ + O_2 \qquad (16b)$$

Analysis of the ratios of product-to-reactant ion signals as function of reagent flows indicates that reactions 13 and 14 reach stationary states. If these are assumed to correspond to chemical equilibria, equilibrium constants of 70 and 6000, respectively, are obtained, which transform to values for ΔG_{298} of -0.11 and -0.22 eV. Furthermore, the hydration reactions 17 and 18 that are evident in Figure 5 approach stationary states with apparent equilibrium constants of 1.9×10^8 and 5.0×10^6, leading to $\Delta G_{298}(17) = -0.5$ eV and $\Delta G_{298}(18) = -0.4$ eV, respectively. Note, however, that formation of $[V,O_6,D_2]^+$ by reaction 14 is ignored in the analysis (see below).

$$[V,O_5]^+ + D_2O \rightarrow [V,O_5]^+\bullet(D_2O) \qquad (17)$$

$$[V,O_5]^+\bullet(D_2O) + D_2O \rightarrow [V,O_5]^+\bullet(D_2O)_2 \qquad (18)$$

Multiple collision-induced dissociation of the $[V,O_n]^+\bullet(D_2O)_m$ ions affords exclusive losses of intact water and/or dioxygen ligands, whereas fragments due to homolytic bond cleavages, such as OH radical losses, are not observed.

Theoretical Results

There are many possible structural isomers for the $[V,O_n]^+$ and $[V,O_n,H_2]^+$ ($n = 1-7$) species observed in the experimental studies. For example, already a system as small as $[M,O_2]^+$ has three conceivable structures: an inserted dioxide with OMO connectivity, a side-on complex with an intact O_2 moiety, and an end-on coordinated O_2 ligand leading to a superoxide-like MOO structure.[31] Earlier calculations for cationic $[M,O_2]^+$ species with M = Cr, Fe, and Cu revealed that the energetic spacings of these isomers vary along the first transition row.[32] Thus, the dioxide is strongly preferred for the early transition metal chromium ($\Delta E = 1.4$ eV),[32b] whereas this preference is reduced for iron ($\Delta E = 0.22$ eV)[32] and even reverses for the late transition metal copper.[32a] Although $[V,O_2]^+$ can safely be assumed to have a dioxide structure,[33] the isomerism of the higher MO_n^+ systems suggests an even larger variety of structures for the $[V,O_n]^+$ ($n = 3-7$) species, because as the number of oxygen atoms coordinated to the vanadium center increases, the formation of O_2 and perhaps even O_3 ligands might become energetically favored. Another structural dichotomy emerges with the formal water complexes $[V,O_n]^+\bullet H_2O$. In these systems, the formation of O−H bonds with the oxygen atoms might be preferred over the presence of an intact water ligand. For example, it has recently been shown that in the $[Fe,O_2,H_2]^+$ system the iron dihydroxide cation $Fe(OH)_2^+$ is 0.65 eV more stable than the hydrated metal oxide cation $OFe(OH_2)^+$.[34] In addition to the structural manifold of the $[V,O_n]^+$ and $[V,O_n,H_2]^+$ species, various electronic states need to be considered, and an intuitive assignment of the ground-state multiplicity is difficult, if not impossible.[26]

To provide insight into the structures of the $[V,O_n]^+$ ($n = 1-7$) and $[V,O_n,H_2]^+$ ($n = 2, 4$) species formed in the experiments, the structures are studied by calculations at the B3LYP level of theory. The results of these calculations are summarized below; with respect to the basic $[V,O,H_2]^+$ system, we refer to the extensive theoretical work performed by Ugalde

TABLE 2: Total Energies (E_{tot}), ZPVE Corrected Energies (E_{corr}), Gibbs Free Energies (G_{298K}), and Entropies (S_{298K}) for Selected Fragments Computed at the B3LYP/TZV Level of Theory

species[a]	state	E_{tot} [Hartree]	E_{corr} [Hartree]	G_{298K} [Hartree]	S_{298K} [cal mol^{-1} K^{-1}]
O	^{3}P	−75.09526		−75.11021	36.4
O_2	$^3\Sigma^-$	−150.38204	−150.37835	−150.39832	49.0
OH	$^2\Pi$	−75.76618	−75.75779	−75.77472	42.6
O_3	$^1A_1$	−225.49798	−225.49080	−225.51392	56.9
H_2O	$^1A_1$	−76.46062	−76.43945	−76.45709	45.1
V^+	^{3}G	−943.58967		−943.60626	39.9
	^{5}D	−943.66852		−943.68560	40.9
V	^{4}F	−943.91013		−943.92700	40.5
	^{6}D	−943.90863		−943.92588	41.3
VO^+	$^3\Sigma^-$	−1018.96687	−1018.96430	−1018.98684	54.4
VO	$^4\Sigma^-$	−1019.23941	−1019.23703	−1019.25989	55.1
VOH^+[b]	^{4}A″	−1019.59150	−1019.58047	−1019.60439	59.5
	^{2}A′	−1019.54573	−1019.53442	−1019.55843	59.7

[a] Selected geometric parameters: O_2, $r_{calc} = 1.21$ vs $r_{exp} = 1.2074$ Å; O_3, $r_{calc} = 1.26$ vs $r_{exp} = 1.2716$ Å and $\alpha_{calc} = 118.3$ vs 117.5°; OH, $r_{calc} = 0.98$ vs $r_{exp} = 0.96966$ Å; H_2O, $r_{calc} = 0.96$ vs $r_{exp} = 0.9575$ Å and $\alpha_{calc} = 105.0$ vs 104.5°; $^3VO^+$, $r = 1.55$ Å; ^4VO, $r = 1.59$ Å; $^4VOH^+$, $r_{VO} = 1.73$ Å, $r_{OH} = 0.97$ Å, $\alpha = 164°$; $^2VOH^+$, $r_{VO} = 1.74$ Å, $r_{OH} = 0.97$ Å, $\alpha = 151°$. [b] $^4VOH^+$ can be considered as a quasi-linear molecule because the linear state VOH^+ ($^4\Sigma^-$), having two imaginary modes is only little higher in energy ($E_{tot} = -1019.59142$) and even more stable when ZPVE is included ($E_{corr} = -1019.58096$).

and co-workers.[16] For the sake of clarity, the presentation is divided into five subsections: (i) fragments, (ii) $[V,O_n]^+$ with $n = 2$ and 3, (iii) $[V,O_4]^+$, (iv) $[V,O_n]^+$ with $n = 5-7$, and (v) $[V,O_n,H_2]^+$ with $n = 2$ and 4.

Fragments. Table 2 summarizes states, energies, and entropies calculated for the monoxides VO and VO^+, the hydroxide cation VOH^+, and the bare vanadium species V and V^+ along with the ligands O, O_2, O_3, OH, and H_2O. The ground-state configurations given for all species in Table 2 reproduce those tabulated in compilations of Moore[11] and Herzberg.[35] The bond lengths of 1.59 and 1.55 Å obtained for VO and VO^+ agree well with experimental values of $r_{VO} = 1.5893$ Å[36] and $r_{VO^+} = 1.5612$ Å.[37] Further, comparison of the geometries calculated for O_2, O_3, OH, and H_2O with tabulated data[36] shows that the calculations yield geometries similar to those established by experiments. The good agreement between the experimental and calculated values suggests that the basis sets suffice for a reasonable description of the systems under investigation. As a note of caution, we shall add, however, that density functional theory does not correctly reproduce the energetics of transition metal oxides in all cases.[29] Specifically, even if the thermochemical properties of the reference fragments are described reasonably well at the chosen level of theory, the energetics of unknown systems bear a certain amount of imponderability. Benchmarking by classical, wave function based ab initio methods can lend further confidence to the results,[38] but is not pursued in the present study.

$[V,O_n]^+$ ($n = 2, 3$). As vanadium monoxide has a $^3\Sigma^+$ ground state, the coupling with the ^{3}P and $^3\Sigma^-$ states of atomic and molecular oxygen, respectively, may give rise to singlet, triplet, and quintet multiplicities in the corresponding $[V,O_n]^+$ ions ($n = 2, 3$). For $[V,O_2]^+$, all three isomers discussed above for the $[M,O_2]^+$ systems are located as minima (Table 3). The inserted dioxide species, designated as $^1VO_2^+$, is found to be the energetically lowest isomer with a C_{2v}-symmetric $^1A_1$ ground state;[39] a C_s-symmetric ^{3}A″ excited state with two different VO bond lengths is 1.39 eV higher in energy. The side-on, $V(O_2)^+$, and end-on, $V(OO)^+$, complexes exhibit $^3B_1$ and $^3\Sigma^-$ ground states and are 1.98 and 2.78 eV, respectively, higher in energy than $^1VO_2^+$. This finding is in good agreement with earlier ground-state assignments and the strong metal-oxide bonds formed by early transition metals.[33] The ground-state geometry (Figure 6) of $^1VO_2^+$ is characterized by two equal V−O bonds that are slightly longer than that calculated for free VO^+ (1.56 vs 1.55 Å) and an OVO angle of 106°. While the side-on $^3V(O_2)^+$ complex has long V−O bonds (1.85 Å), a 10% elongation of the O−O moiety (compared to free $^3O_2$) points to more than a mere electrostatic interaction of the O_2 ligand with the V^+ center. In contrast, the O−O bond length in the end-on $^3V(OO)^+$ complex is almost undisturbed, suggesting a predominating electrostatic interaction, which is in agreement with the lower stability of the end-on complex and the oxophilicity of vanadium. The preference for triplet states in the O_2-ligated V^+ cations can be rationalized easily by the different bonding schemes. In $^1VO_2^+$, perfect pairing of the four d electrons of V^+ (^{5}D) with the four electrons provided by the two O atoms (^{3}P) leads to a singlet, whereas end-on and side-on combinations of the two unpaired electrons of triplet O_2 ($^3\Sigma^-$) with V^+ in a perfect-pairing fashion lead to triplet states.

The lower half of Figure 6 displays the computed geometries of the $[V,O_3]^+$ isomers. The presence of three O atoms also allows for the formation of a new oxygen ligand, i.e., ozone, suggesting the possible existence of $V(O_3)^+$ complexes. As can be seen in the lower half of Table 3, all isomers prefer triplet ground states. The energies given for the quintet species are derived from single-point calculations, i.e., vertical excitation at the minimum geometries of the ground states (here, triplets) to the quintet surface. Because the single-point calculations result in energies much higher than those of the singlet and triplet species, no further geometry optimizations of the quintet geometries seem necessary.

The isomer with the lowest energy demand is the C_s-symmetric $^3OV(O_2)^+$ complex, which can be visualized as a $^3VO^+$ cation with a side-on coordinated O_2 ligand. This description of $^3OV(O_2)^+$ is consistent with the shortening of r_{OO} by 0.04 Å concomitant with elongation of r_{VO} by 0.08 Å in comparison with $^3V(O_2)^+$ (see above). Interestingly, $OV(O_2)^+$ has a triplet ground state rather than the perfect-pairing singlet configuration intuitively expected for an oxovanadium(V) peroxide cation. The computed geometry of the singlet is in accordance with this description, i.e., shortened V−O bonds along with an elongated O−O distance. However, $^1OV(O_2)^+$ is located 0.59 eV above the triplet ground state. The next higher isomer ($E_{rel} = 0.89$ eV) is the planar $OV(OO)^+$ complex (^{3}A′) with the O_2 ligand in an end-on coordination. The trioxide structure $^3VO_3^+$ with a ^{3}A″ ground state is located at $E_{rel} = 1.11$ eV and has one short and two longer V−O bonds ($r_{VO} = 1.56$ and 1.72 Å). The longer bonds point to formation of two V−O single bonds, leaving a free electron on each of the two oxygen atoms. The latter nicely rationalizes the preference of the $[V,O_3]^+$ system to form a structure with an O_2 moiety by forming a bond between two singly bonded oxygen atoms. The fourth isomer investigated is the ozone complex $^3V(O_3)^+$ at $E_{rel} = 2.74$ eV in which all three oxygen atoms are in the same hemisphere of the V^+ center. On the singlet surface, only a saddle point ($\nu = i421$ cm^{-1}) could be located for $^1V(O_3)^+$, and IRC calculations reveal this structure to be a transition structure for the degenerate rearrangement of the singlet, i.e., O atom exchange between ^{1}**O**$V(O_2)^+$ and $^1OV($**O**$O)^+$.

$[V,O_4]^+$. Six conceivable structural isomers are expected for species with the formula $[V,O_4]^+$ on the basis of the possible addition of an O_2 molecule to the three isomers found for the $[V,O_2]^+$ system or a single O atom to the four isomers found

TABLE 3: Total Energies (E_{tot}), ZPVE Corrected Energies (E_{corr}), Gibbs Free Energies (G_{298K}), Entropies (S_{298K}), and Relative Energies (E_{rel}) of $[V,O_n]^+$ Species with $n = 2$ and 3 Computed at the B3LYP/TZV Level of Theory (lowest lying isomers in bold)

species[a]	state	E_{tot} [Hartree]	E_{corr} [Hartree]	G_{298K} [Hartree]	S_{298K} [cal mol^{-1} K^{-1}]	E_{rel}[a] [eV]
VO_2^+	**$^1A_1$**	**−1094.20168**	**−1094.19556**	**−1094.22053**	**61.2**	**0.00**
	$^3A''$	−1094.14923	−1094.14465	−1094.17180	66.5	1.39
	$^5A_2$	−1094.06311	−1094.06311	−1094.08659	66.3	3.60
$V(O_2)^+$	$^1A_1$	−1094.07699	−1094.07177	−1094.09669	61.1	3.37
	$^3B_1$	−1094.12717	−1094.12285	−1094.14912	64.7	1.98
	$^5B_2$	−1094.10872	−1094.10368	−1094.13036	65.1	2.50
$V(OO)^+$	$^1\Sigma^+$	−1094.03025	−1094.02445	−1094.04832	59.6	4.66
	$^3\Sigma^-$	−1094.09825	−1094.09334	−1094.11880	63.7	2.78
	$^5A''$	−1094.08441	−1094.08029	−1094.10763	67.4	3.14
$OV(O_2)^+$	$^1A'$	−1169.37646	−1169.36755	−1169.39501	68.6	0.59
	$^3A''$	**−1169.39824**	**−1169.38931**	**−1169.41793**	**71.3**	**0.00**
	^5sp[b]	−1169.26196				3.71[c]
$OV(OO)^+$	$^1A'$	−1169.34227	−1169.33275	−1169.36056	69.0	1.54
	$^3A'$	−1169.36385	−1169.35655	−1169.38773	79.0	0.89
	^5sp[b]	−1169.31146				2.32[c]
VO_3^+	^1E	−1169.30626	−1169.29946	−1169.32655	69.0	2.44
	$^3A''$	−1169.35516	−1169.34861	−1169.37771	73.2	1.11
	^5sp[b]	−1169.26185				3.71[c]
$V(O_3)^+$	$^1A'$[d]	−1169.24644	−1169.23941	−1169.26648	67.0	4.08
	$^3A''$	−1169.29654	−1169.28870	−1169.31703	70.4	2.74
	^5sp[b]	−1169.22274				4.75[c]

[a] 0 K values with respect to the lowest $[V,O_n]^+$ isomer of each *n*. [b] Energy obtained upon vertical excitation from the energetically lowest spin state to the quintet surface. [c] ZPVE neglected. [d] Transition stucture at this level of theory.

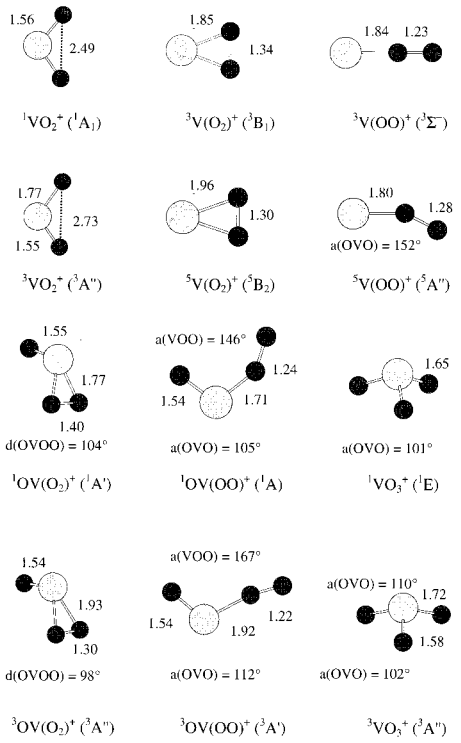

Figure 6. Geometries computed for several isomers of $[V,O_2]^+$ and $[V,O_3]^+$; bond lengths in Ångstrøm and angles in degree.

for the $[V,O_3]^+$ system. Five of these are located using the theoretical approach chosen here. Consistent with neutral and anionic $[V,O_4]$ species,[2,3] the most stable isomer bears a dioxide structure with an end-on coordinated O_2 ligand (Table 4). The long distance between the O_2 ligand and the VO_2^+ core and the undisturbed O−O bond indicates the presence of a weak electrostatic interaction between VO_2^+ and the O_2 ligand (Figure 7). The lowest electronic state for the $O_2V(OO)^+$ complex is a C_1 symmetric triplet state with a $^1A'$ state 1.36 eV higher in energy. The preference of the $O_2V(OO)^+$ complex for a triplet multiplicity is easily rationalized by the $^1A_1$ and $^3\Sigma^-$ ground states of VO_2^+ and O_2, respectively. The next higher isomer ($\Delta E_{rel} = 1.31$ eV) is the $OV(O_3)^+$ complex composed of a VO^+ ion ligated by an ozone ligand. Here, the $^1A'$ state is more stable than the $^3A'$ state by 0.29 eV, indicating that on the singlet surface the ozone ligand is stabilized by the additional oxygen ligand on the V^+ center. The ^3A ground state of the $[V,O_4]^+$ isomer with two side-on coordinated oxygen moieties is found at $E_{rel} = 1.63$ eV, with the ^5A and ^1A states at 1.83 and 2.04 eV, respectively. The two oxygen moieties are slightly rotated with respect to each other on all three spin surfaces, leading to C_1 symmetries for the $V(O_2)_2^+$ complexes. The V−O and O−O bond lengths of $V(O_2)_2^+$ are similar to those of the side-on $V(O_2)^+$ complexes (see above). Combination of end-on and side-on coordination of O_2 units to V^+ as present in the $V(O_2)(OO)^+$ species leads to a $^3A''$ state at $E_{rel} = 2.15$ eV. The last isomer investigated is the tetroxide VO_4^+. For this geometry, stationary points are found only on the triplet and quintet potential energy surfaces at energies of 3.18 (^3A) and 3.33 eV ($^5A'$), respectively, above the $^3O_2V(OO)^+$ ground state. All calculations on the singlet surface always converge to $^1O_2V(O_2)^+$. The latter finding can be rationalized by taking the electrons involved in the bonding into consideration. V^+ (^5D) has four 3d electrons, and each O atom has two unpaired electrons. Assuming equal bonding for all four O ligands, the number of valence electrons on the V^+ center is used up by formation of four V−O single bonds, and each of the oxygen ligands is left over with one unpaired electron. To achieve a singlet multiplicity in this system, two of the electrons have to have opposite spin, resulting in an highly energetic open-shell singlet as is emphasized by the 6.93 eV needed for the vertical excitation from the triplet to the singlet surface. However, the proximity of the oxygen atoms favors the formation of O−O bonds, leading to the much more stable $^1O_2V(OO)^+$.

$[V,O_n]^+$ ($n = 5-7$). From the results presented in the previous subsections, we can conclude that with an increasing number of oxygen atoms coordinated to the V^+ center there is a clear preference for formation of O_2 and O_3 ligands. Accord-

TABLE 4: Total Energies (E_{tot}), ZPVE Corrected Energies (E_{corr}), Gibbs Free Energies (G_{298K}), Entropies (S_{298K}), and Relative Energies (E_{rel}) of $[V,O_4]^+$ Species Computed at the B3LYP/TZV Level of Theory (lowest lying isomers in bold)

species[a]	state	E_{tot} [Hartree]	E_{corr} [Hartree]	G_{298K} [Hartree]	S_{298K} [cal mol^{-1} K^{-1}]	E_{rel}[a] [eV]
$O_2V(O_2)^+$	^{1}A′	−1244.56419	−1244.55271	−1244.58438	81.9	1.36
	^{3}A″	**−1244.61418**	**−1244.60279**	**−1244.63713**	**87.9**	**0.00**
	sp	−1244.54569				1.86
$OV(O_3)^+$	^{1}A′	−1244.55636	−1244.54396	−1244.57260	72.7	1.31
	^{3}A′	−1244.56634	−1244.55461	−1244.58479	76.7	1.60
	^{5}sp[b]	−1244.44514				4.61[c]
$V(O_2)_2^+$	^{1}A	−1244.53959	−1244.52770	−1244.55700	74.7	2.04
	^{3}A	−1244.55363	−1244.54274	−1244.57418	80.5	1.63
	^{5}A	−1244.54696	−1244.53567	−1244.56741	80.9	1.83
$V(O_2)(OO)^+$	^{1}A	−1244.49835	−1244.48603	−1244.51565	75.5	3.18
	^{3}A″	−1244.53445	−1244.52380	−1244.55589	82.7	2.15
	^{5}sp[b]	−1244.50912				2.84[c]
VO_4^+	^{1}sp[d]	−1244.35585				6.93[c]
	^{3}A	−1244.49388	−1244.48607	−1244.51819	83.7	3.18
	^{5}A′	−1244.49055	−1244.48052	−1244.51380	87.0	3.33

[a] 0 K values with respect to the lowest $[V,O_4]^+$. [b] Energy obtained upon vertical excitation from the energetically lowest spin state to the quintet surface. [c] ZPVE neglected. [d] Single point energy on the singlet surface. Upon optimization, the VO_4^+ geometry converges to the $VO_2(O_2)^+$ isomer.

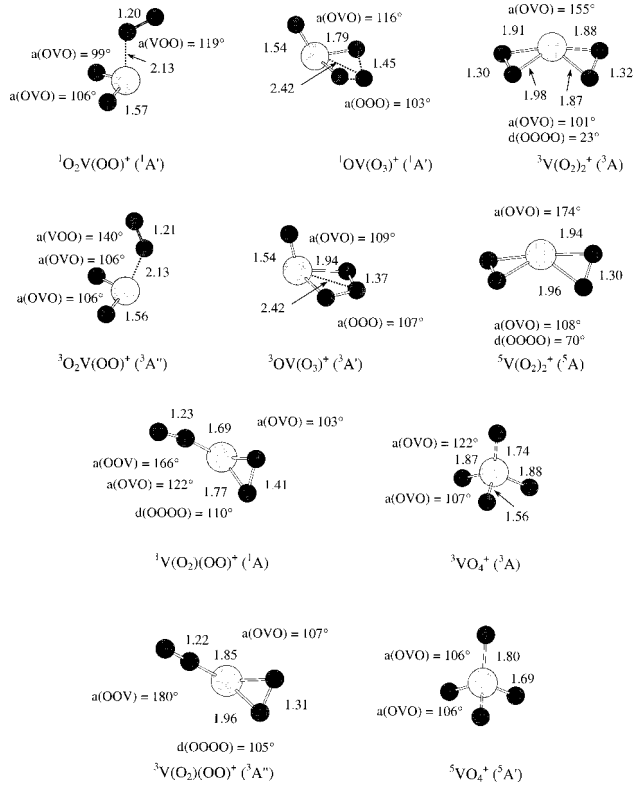

Figure 7. Geometries computed for several isomers of $[V,O_4]^+$; bond lengths in Ångstrøm and angles in degree.

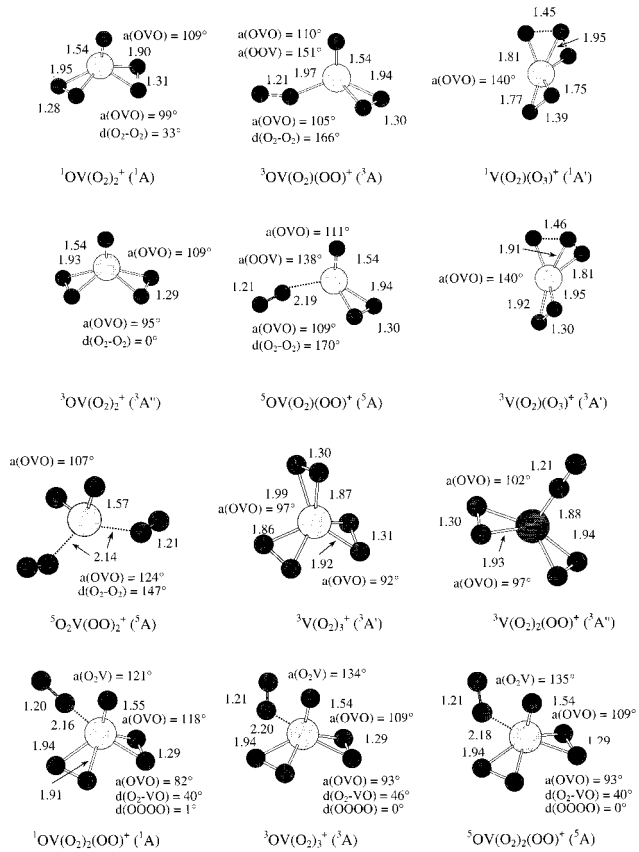

Figure 8. Geometries computed for selected isomers of $[V,O_5]^+$, $[V,O_6]^+$, and $[V,O_7]^+$; bond lengths in Ångstrøm and angles in degree.

ingly, only the $[V,O_5]^+$ isomers shown in Figure 8 are considered.[40] The energetically lowest isomer is the $OV(O_2)_2^+$ complex with a ^{3}A″ ground state and an ^{1}A excited state (Table 5). According to its geometry, this complex can be understood as a VO^+ cation ligated by two equal O_2 units. The next higher isomer is a C_1 symmetric quintet state found at $E_{rel} = 0.53$ eV, which may be described as a VO^+ cation coordinated by a side-on and an end-on O_2 ligand. The corresponding triplet state has a similar structure and is located at $E_{rel} = 0.80$ eV; not surprisingly, the singlet $^1OV(O_2)(OO)^+$ complex is much higher in energy. The last isomer located is the $V(O_2)(O_3)^+$ complex, which can be described as a V^+ ion coordinated by O_2 and O_3 moieties. $V(O_2)(O_3)^+$ exhibits a ^{1}A′ ground state at $E_{rel} = 2.79$ eV with a ^{3}A′ state very close in energy ($\Delta E_{rel} = 0.06$ eV).

Although $[V,O_6]^+$ is not observed in the experiments, it is included in the theoretical treatment for the sake of completeness. Not surprisingly, the most stable species can be described as a vanadyl cation $^1VO_2^+$ coordinated to two end-on O_2 ligands in a high-spin fashion. The corresponding triplet $O_2V(OO)_2^+$ (^{3}A) is 0.43 eV above the ground state, whereas all other species studied are much higher in energy. Addition of an O_2 ligand to the $OV(O_2)_2^+$ complexes leads to the $OV(O_2)_3^+$ isomers shown in Figure 8. Vanadium is no longer able to coordinate all O_2 ligands in a side-on fashion. Therefore, one of the O_2 ligands binds only with one oxygen in an end-on fashion. These findings are in good agreement with a hexa-coordination preferred by

TABLE 5: Total Energies (E_{tot}), ZPVE Corrected Energies (E_{corr}), Gibbs Free Energies (G_{298K}), Entropies (S_{298K}), and Relative Energies (E_{Rel}) of $[V,O_n]^+$ Species with $n = 5-7$ Computed at the B3LYP/TZV Level of Theory (lowest lying isomers in bold)

species[a]	state	E_{tot} [Hartree]	E_{corr} [Hartree]	G_{298K} [Hartree]	S_{298K} [cal mol^{-1} K^{-1}]	E_{rel}[a] [eV]
$OV(O_2)_2^+$	^{1}A	−1319.75019	−1319.73518	−1319.76615	81.1	2.06
	^{3}A″	**−1319.82677**	**−1319.81080**	**−1319.84241**	**81.8**	**0.00**
	^{5}sp[b]	−1319.73421				2.52[c]
$OV(O_2)(OO)^+$	^{1}A′	−1319.74405	−1319.72971	−1319.76219	85.5	2.21
	^{3}A	−1319.79577	−1319.78148	−1319.81534	88.8	0.80
	^{5}A	−1319.80541	−1319.79125	−1319.82658	92.5	0.53
$V(O_2)(O_3)^+$	^{1}A′	−1319.72377	−1319.70824	−1319.73852	78.1	2.79
	^{3}A′	−1319.72011	−1319.70615	−1319.73755	80.4	2.85
	^{5}sp[b]	−1319.62422				5.46[c]
$V(O_2)_3^+$	^{1}A	−1394.92476	−1394.90556	−1394.93727	83.6	2.78
	^{3}A′	−1394.98433	−1394.96696	−1395.00152	91.7	1.11
	^{5}A′	−1394.96678	−1394.94939	−1394.98470	93.5	1.58
$V(O_2)_2(OO)^+$	^{1}sp[b]	−1394.87168				4.15[c]
	^{3}A″	−1394.96882	−1394.95218	−1394.98780	95.4	1.51
	^{5}A	−1394.94964	−1394.93328	−1394.97000	97.9	2.02
$O_2V(OO)_2^+$	^{1}sp[b]	−1394.92127				2.80[c]
	^{3}A	−1395.00831	−1394.99173	−1395.03138	106.2	0.43
	^{5}A	**-1395.02419**	**-1395.00758**	**-1395.04693**	**105.5**	**0.00**
$OV(O_2)_3^+$	^{1}A	−1470.12678	−1470.10553	−1470.14152	97.7	2.90
	^{3}A	−1470.23266	−1470.21138	−1470.24868	100.8	0.02
	^{5}A	**-1470.23320**	**-1470.21201**	**-1470.24970**	**101.6**	**0.00**

[a] 0 K values with respect to the lowest $[V,O_n]^+$ isomer of each n. [b] Energy obtained upon vertical excitation from the energetically lowest spin state to the quintet surface. [c] ZPVE neglected.

TABLE 6: Total Energies (E_{tot}), ZPVE Corrected Energies (E_{corr}), Gibbs Free Energies (G_{298K}), Entropies (S_{298K}), and Relative Energies (E_{rel}) of $[V,O_n,H_2]^+$ Species with $n = 2$ and 4 Computed at the B3LYP/TZV Level of Theory (lowest lying isomers in bold)

species[a]	state	E_{tot} [Hartree]	E_{corr} [Hartree]	G_{298K} [Hartree]	S_{298K} [cal mol^{-1} K^{-1}]	E_{rel}[a] [eV]
$^3VO^+ + H_2O$	^{1}A′	−1095.42749	−1095.40375	−1095.44346	99.5	2.34
$OV(OH_2)^+$	^{1}A′	−1095.46281	−1095.43511	−1095.46281	70.5	1.48
	^{3}A″	−1095.49803	−1095.47082	−1095.50011	74.3	0.51
	^{5}sp[b]	−1095.35316				4.42[c]
TS	^{1}A	−1095.38809	−1095.36544	−1095.39177	65.2	3.38
	^{3}A	−1095.42835	−1095.40585	−1095.43328	67.6	2.27
	sp[b]	−1095.33074				5.03[c]
$V(OH)_2^+$	$^1\Sigma^+$	−1095.47586	−1095.45003	−1095.47857	73.2	1.07
	$^3\Sigma^-$	**−1095.51545**	**−1095.48949**	**−1095.51696**	**70.6**	**0.00**
	^{5}sp[b]	−1095.38322				3.60[c]
$^4VOH^+ + {}^2OH$		−1095.35768	−1095.33826	−1095.37911	102.1	4.12[c]
$OV(OH_2)(O_2)^+$	^{1}A′	−1245.93166	−1245.89737	−1245.92829	81.3	0.49
	^{3}A	−1245.94186	−1245.90791	−1245.94074	86.1	0.20
	^{5}sp[b]	−1245.81283				3.64[c]
$V(OH)_2(O_2)^+$	^{1}A	−1245.93529	−1245.90342	−1245.93386	80.3	0.32
	^{3}A″	**−1245.94654**	**−1245.91524**	**−1245.94756**	**85.4**	**0.00**
	^{5}sp[b]	−1245.81564				3.56[c]

[a] 0 K values with respect to the lowest isomer of each group. [b] Energy obtained upon vertical excitation from the energetically lowest spin state to the quintet surface. [c] ZPVE neglected.

the simplest vanadyl complex $O_2V(OH_2)_4^+$ formed upon dissolving V_2O_5 in acidic solutions.[41]

$[V,O_n,H_2]^+$ ($n = 2, 4$). In the experiments, $[V,O_n,H_2]^+$ cations are formed either by addition of water to $[V,O_{n-1}]^+$ ions or by O_2/water exchange of $[V,O_{n+1}]^+$ species. It is interesting to ask whether these ions correspond to hydrated vanadium oxides or if they can undergo interconversion to the corresponding dihydroxide ions. To evaluate the latter, we have chosen the smallest system possible consisting of VO^+ and H_2O. A ^{3}A″ ground state is found for $OV(OH_2)^+$ ($E_{rel} = 0.51$ eV) with the ^{1}A′ excited state at $E_{rel} = 1.5$ eV (Table 6). As can be seen in Figure 9, the geometry of the water ligand is almost undisturbed compared to free H_2O, indicating that the interaction is predominantly electrostatic. The dihydroxide species $V(OH)_2^+$ corresponds to the global minimum with a $^3\Sigma^-$ ground state and a $^1\Sigma^+$ excited state ($\Delta E_{rel} = 1.1$ eV), both with linear geometries and in good agreement with earlier calculations of Ricca and Bauschlicher.[42] In analogy to the corresponding $[Fe,O_2,H_2]^+$ system,[26b,34] the vanadium dihydroxide cation is found to be 0.5 eV more stable than the water complex of VO^+. On both spin surfaces, the transition structures (TSs) for the interconversion of both isomers are characterized by single imaginary frequencies of i1812 and i1928 cm^{-1} for ^{1}TS and ^{3}TS, respectively, which are assigned to 1,3-H shifts from the water to the oxygen ligand. Energetically, singlet and triplet surfaces are almost alike except that the singlet surface is about 1 eV higher in energy throughout.

Figure 10 and the lower half of Table 6 summarize the results for the $[V,O_4,H_2]^+$ system. Addition of an O_2 unit to the $[V,O_2,H_2]^+$ system does not induce dramatic changes in the overall picture but results in a closer energetic spacing of the two isomers and their different spin multiplicities. The dihy-

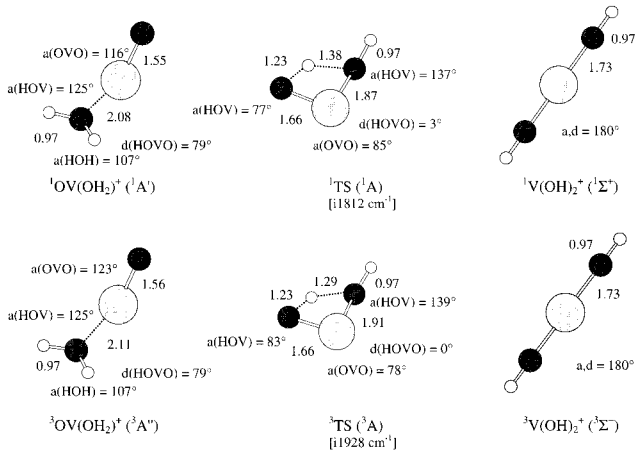

Figure 9. Geometries computed for $OV(OH_2)^+$, $V(OH)_2^+$, and the associated transition structures; bond lengths in Ångstrøm and angles in degree.

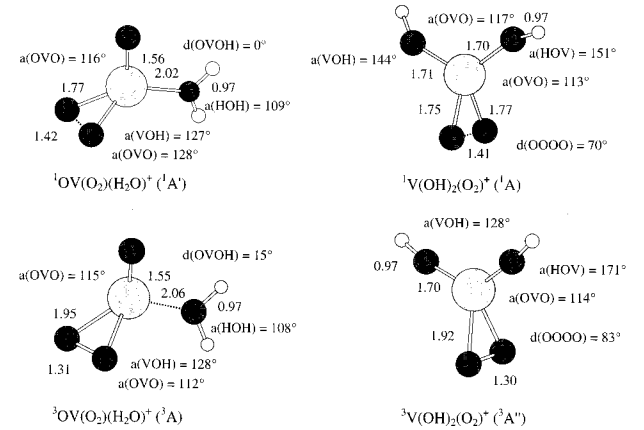

Figure 10. Geometries computed for the $[V,O_4,H_2]^+$ system; bond lengths in Ångstrøm and angles in degree.

droxide complex, $V(OH)_2(O_2)^+$, is again found most stable with a $^3A''$ ground state and a close-lying ^1A excited state (E_{rel} = 0.3 eV). The linear geometries are disturbed by the additional O_2 ligand, leading to a bending of the two OH ligands toward each other. In contrast, minute changes in geometry are observed between $OV(OH_2)^+$ and the corresponding $OV(OH_2)(O_2)^+$ complex. The only notable difference is the alignment of the water ligand relative to the V−O bond, i.e., perpendicular in $OV(OH_2)^+$ and parallel in $OV(OH_2)(O_2)^+$. The ground state of the $OV(OH_2)(O_2)^+$ complex is ^3A (E_{rel} = 0.2 eV) with the ^1A state only 0.3 eV higher in energy.

Discussion

Let us begin with a comprehensive discussion of the calculated energetics, wherein we assume that only the lowest-lying isomers and/or states are relevant with respect to the experiments (Table 7). As far as the $[V,O_n]^+$ cations are concerned, the data suggest that dioxygen complexes rather than low-spin coupled peroxides are formed upon association of molecular oxygen to VO^+ in the gas phase. The computed sequential bond energies for the first two dioxygen ligands show only a small decrease from $D_0(OV^+-O_2)$ = 1.27 eV to $D_0(OV(O_2)^+-O_2)$ = 1.17 eV, whereas the third dioxygen ligand in $[V,O_7]^+$ is more weakly bound, $D_0(OV(O_2)_2^+-O_2)$ = 0.62 eV. The corresponding rate constants measured experimentally for the consecutive associations of VO^+ with O_2 are $k_{10} = 2.0 \times 10^{-13}$ cm^3 molecule^{-1} s^{-1}, $k_{11} = 7.3 \times 10^{-12}$ cm^3 molecule^{-1} s^{-1}, and $k_{12} = 2.0 \times 10^{-12}$ cm^3 molecule^{-1} s^{-1}. The remarkable increase by more than an order of magnitude from k_{10} to k_{11} can be attributed to the increase of the lifetime of the corresponding association complexes with increasing molecular size. Thus, although the binding energies are similar, association of VO^+ with O_2 involves six degrees of freedom, whereas twice as many are available for $[V,O_5]^+$. An increased lifetime of the encounter complex favors termolecular stabilization with the helium buffer gas, and this accounts for the significant increase of the apparent rate constant. For the third association, two effects compete with each other: whereas the density of states increases further, the binding energy shrinks to about half of that for the two first oxygen ligands. Compensation leads to an intermediate value for k_{12}. Hence, the experimental results are qualitatively consistent with the computationally predicted $OV(O_2)_m^+$ structures of the $[V,O_n]^+$ ions (with $m = 1-3$ and $n = 2m + 1$, respectively). Description of the $[V,O_n]^+$ ions as dioxygen complexes is further supported by the observed ligand-switching reaction with water. In agreement with the experimental findings, the computations predict $D_0(OV^+-OH_2)$ = 1.83 eV and $D_0(OV(O_2)^+-OH_2)$ = 2.15 eV for bonding of the water ligand in the hydrated ions, which are much larger than the binding energies of the corresponding dioxygen complexes (see above). This situation is complemented with the observation that the $[V,O_5]^+$ and $[V,O_7]^+$ species undergo exchange reactions in competition with association to yield the corresponding hydrated ions, which then continue to cluster with water. In marked contrast, association of the diatomic VO^+ cation with either O_2 or H_2O occurs very slowly, quite obviously due to the low number of degrees of freedom available.

The behavior of $[V,O_3]^+$ deserves more detailed consideration. In the presence of only oxygen in the helium flow (Figures 3 and 4), the loss of $[V,O_3]^+$ is rate-limited by its production from VO^+, giving rise to a quasi-stationary ion abundance in the percent range. As outlined above, this behavior can be explained by the different rates for formation ($k_{10} = 2.0 \times 10^{-13}$ cm^3 molecule^{-1} s^{-1}) and subsequent association ($k_{11} = 7.3 \times 10^{-12}$ cm^3 molecule^{-1} s^{-1}) of this ion. Theory predicts $^3OV(O_2)^+$ to be the most stable $[V,O_3]^+$ isomer, with binding characteristics of an dioxygen complex and a computed binding

TABLE 7: Bond Dissociation Energies (D_0 at 0 K) for Ground-State Vanadium Species (in kcal mol^{-1}) Calculated at the B3LYP/TZp Level of Theory[a] and Some Literature Data Given for Comparison

species	state	bond	D_0	other values
VO^+	$^3\Sigma^-$	V^+-O	125.9	138.1[b]
VO_2^+	$^1A_1$	OV^+-O	85.3	70.6[c]/90.2[d]
$OV(O_2)^+$	$^3A''$	OV^+-(O_2)	29.3	
$O_2V(O_2)^+$	^3A	O_2V^+-(O_2)	18.1	
$OV(O_2)_2^+$	$^3A''$	$(O_2)OV^+$-(O_2)	27.1	
$O_2V(O_2)_2^+$	^5A	$O_2V(O_2)^+$-(O_2)	14.3	
$OV(O_2)_3^+$	^5A	$(O_2)_2OV^+$-(O_2)	14.3	
VOH^+	$^4A''$	V^+-OH	96.7	103.8[e]/98.6[f]
$OV(OH_2)^+$	$^3A''$	OV^+-OH_2	42.1	
$V(OH)_2^+$	$^3\Sigma^-$	HOV^+-OH	94.9	100.6[f]
$OV(OH_2)(O_2)^+$	^3A	$(H_2O)OV^+-O_2$	36.9	
		$(O_2)OV^+-OH_2$	49.7	
$V(OH)_2(O_2)^+$	$^3A''$	$O_2-V(OH)_2^+$	29.7	

[a] If desired, the values can be converted into heats of formation at 0 or 298 K using $\Delta H_{f,0K}(VO^+)$ = (198.8 ± 3) kcal mol^{-1} and $\Delta H_{f,298K}(VO^+)$ = (197.4 ± 3) kcal mol^{-1} as absolute anchors in combination with literature thermochemistry. [b] Experimental D_0, see ref 21. [c] Experimental D_0, see: Sievers, M. R.; Armentrout, P. B. *J. Chem. Phys.* **1995**, *102*, 754. [d] Calculated D_0, see ref 33 for a discussion. [e] Taken from: Armentrout, P. B.; Kickel, B. L. In *Organometallic Ion Chemistry*; Freiser, B. S., Ed.; Kluwer: Dordrecht, 1996; p 1. [f] Best theoretical estimate taken from ref 42.

energy of $D_0(OV^+-O_2) = 1.27$ eV, which is substantially smaller than $D_0(OV^+-OH_2) = 1.83$ eV. Thus, occurrence of the exchange reaction 16b is predicted by theory. However, Figure 5 implies that $[V,O_3]^+$ does not react rapidly with water, and specifically the anticipated ligand-exchange product $[V,O_2,D_2]^+$ is observed only in trace amounts. Accordingly, both the association according to reaction 16a as well as the ligand-exchange reaction 16b have very small rate constants, if occurring at all, under SIFT conditions.

$$^3OV(O_2)^+ + {}^1H_2O \rightarrow {}^3OV(OH_2)^+ + {}^3O_2 \qquad (19)$$

To be more specific, the lowest-lying states are considered, i.e., reaction 19. B3LYP predicts ligand exchange to be energetically favorable by 0.56 eV at 0 K, and the predicted $\Delta G_{298}(19) = -0.64$ eV is even slightly larger. Thus, theory suggests that reaction 16b is indeed expected to be a significant product channel. Although inefficient association may be accepted, the failure of reaction 19 is unexpected on the basis of the computed binding energies of VO^+ for water and oxygen ligands, respectively. There are several possible reasons for this behavior. (i) Ligand-exchange according to reaction 19 may be associated with a considerable barrier that prevents the process from occurring at thermal energies. However, the structural characteristics of the triplet ground states of $^3OV(O_2)^+$ and $^3OV(O_2)(H_2O)^+$ give no indications for an origin of such a barrier. (ii) Because of an inbalanced description of correlation energy in cationic transition metal oxides,[29] the DFT calculations may substantially underestimate the stability of the singlet coupled peroxide $^1OV(O_2)^+$, which is computed to be ca. 0.6 eV above $^3OV(O_2)^+$ at the level of theory applied. If the singlet species is indeed lower lying, its contribution to the $[V,O_3]^+$ channel could well give rise to a kinetic hindrance of reaction 19, considering the required change in spin multiplicity and the significantly different structure of $^1OV(O_2)^+$ compared to $^3OV(O_2)^+$. (iii) Another explanation of the discrepancies is that, for some reason, binding to the dipolar water ligand is exaggerated by the DFT approach in comparison to the dioxygen ligand. (iv) Whereas the previous points doubt the reliability of the calculations, the interpretation of the experimental data is not unambiguous in this case. Thus, analysis of what obviously is a termolecular process by an apparent rate constant in terms of a bimolecular process is not necessarily correct. Further, rapid clustering with water and/or oxygen may mask the $[V,O_2,D_2]^+$ channel. Obviously, it is desirable to further probe the chemistry of the $[V,O_3]^+$ ion. Experimentally, however, this is made rather difficult by the unfavorable ratio of k_{10} and k_{11} which limits the amount of $[V,O_3]^+$ formed to about a percent of the overall ion current. In addition, a more elaborated theoretical study of $[V,O_3]^+$ using sophisticated wave function based methods is indicated.

Let us also comment upon the equilibrium constants derived from the SIFT experiments with O_2 and H_2O (Figure 5). Consecutive association of the $[V,O_n]^+$ ions with O_2 and water as well as the competing ligand-exchange processes give rise to a rather complex kinetic situation. In such a case, quasi-stationary states rather than equilibria might be established. For example, the SIFT data used to derive the equilibrium constants for reactions 13 and 17, i.e., involve the $[V,O_5]^+$ precursor for both reactions. Moreover, the putative products may not be formed exclusively from $[V,O_5]^+$ but also via association of $[V,O_3]^+$ with water, ligand exchange of $[V,O_7]^+$ with water, etc. Therefore, it is uncertain whether true equilibria are really established in these experiments. This skepticism is supported by the theoretical results. Thus, the DFT calculations predict

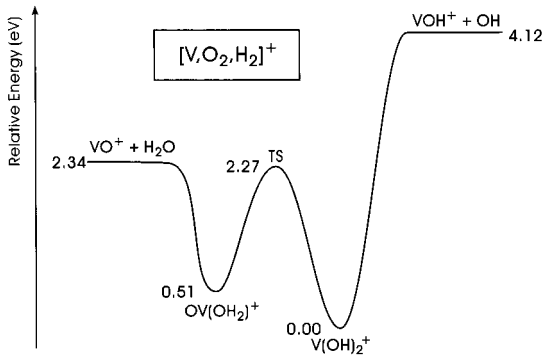

Figure 11. Schematic triplet potential energy surface of the $[V,O_2,H_2]^+$ system.

reaction 13 to be much more exothermic ($\Delta G_{298} = -1.07$ eV) than implied by $K_{eq}(13) = 70$ which suggests $\Delta G_{298} = -0.11$ eV according to the SIFT data.

Finally, let us address the nature of the $[V,O_n,H_2]^+$ species formed in the different experiments. While theory predicts the dihydroxide structure $^3V(OH)_2^+$ to be considerably more stable than the hydrated oxide ion $^3OV(OH_2)^+$, the barrier associated with intramolecular 1,3-hydrogen migration is substantial (Figure 11). In fact, even the lowest-lying ^3TS is close to the asymptote of the reactants, i.e., only 0.07 eV below $^3VO^+ + {}^1H_2O$ at 0 K. This result can be correlated with the slow occurrence of $^{16}O/^{18}O$ exchange in reaction 7. As changes in spin multiplicities do not seem to play a role, the experimental data can be used to roughly estimate the barrier height. As an upper limit, we may assume that the ratio of the measured rate constant k_7 to the respective collision rate obeys an Arrhenius formalism, i.e., $E_{rel}(^3TS) = RT \ln(k_7/k_{c,7})$, where $E_{rel}(^3TS)$ is the energy of TS relative to the $^3VO^+ + {}^1H_2O$ asymptote, $k_7 = (5 \pm 2) \times 10^{-13}$ cm^3 molecule^{-1} s^{-1}, $k_{c,7} = 1.3 \times 10^{-9}$ cm^3 molecule^{-1} s^{-1}, and T is assumed to be 298 K. This approach suggests a barrier of less than 0.2 eV above the entrance channel. On the other hand, $E_{rel}(^3TS)$ cannot be much below the entrance channel, as much more rapid exchange is otherwise expected. For example, $^{16}O/^{18}O$ exchange occurs with a rate constant of ca. 1×10^{-10} cm^3 molecule^{-1} s^{-1} in the FeO^+/H_2O system, where the relevant TS is situated ca. 0.6 eV below the isolated reactants.[26] Accordingly, the predicted barrier height of -0.07 eV in the $[V,O_2,H_2]^+$ system is nicely consistent with the experimental findings. This line of reasoning suggests that the long-lived $[V,O_2,H_2]^+$ species formed by either radiative and/or collisional stabilization correspond to $OV(OH_2)^+$ rather than the more stable $V(OH)_2^+$ isomer. Likewise, generation of $OV(OH_2)^+$ appears likely in the SIFT experiments considering the high amount of buffer gas present in these experiments. Multiple collisions occurring in the flow tube may, however, lead to the formation of the more stable dihydroxide species via intermolecular mechanisms. Specifically, the energy demanding intramolecular 1,3-hydrogen migration may be circumvented by active participation of another water molecule via a proton-shuttle mechanism,[43] according to reaction 20.

$$OV(OH_2)^+ + H_2O \rightarrow V(OH)_2^+ + H_2O \qquad (20)$$

Direct evidence in support of this suggestion is the more rapid $^{16}O/^{18}O$ exchange observed for the long-lived $[V,^{16}O,^{18}O,H_2]^+$ ion; i.e., precisely that result which gives rise to the seemingly contradicting interpretations of the labeling experiments mentioned above. If, however, we assume almost exclusive formation of $OV(OH_2)^+$ in strictly bimolecular collisions, but facile

formation of the more stable $V(OH)_2^+$ ion upon interaction with *another* water molecule, all experimental and theoretical results are in harmony. Following these arguments implies, however, that the kinetic analysis of the association of VO^+ with water according to reaction 3 in terms of radiative and termolecular stabilization mechanisms must be considered as a rough approximation only,[44] because it neglects the existence of two low-lying $[V,O_2,H_2]^+$ isomers and the catalyzing effect of water in reaction 20.

Conclusions

Atomic vanadium cation is rapidly oxidized to VO^+ in the presence of molecular oxygen. The monoxide cation, however, reacts inefficiently with oxygen, water, and several other neutral substrates.[18b] The only reactions observed in the SIFT experiments are consecutive associations with dioxygen to yield first $[V,O_3]^+$, then $[V,O_5]^+$, and then $[V,O_7]^+$ as the final product at room temperature; under ICR conditions, no consecutive reactions of VO^+ with O_2 are observed at all. Density functional theory describes these $[V,O_n]^+$ ions as species having a VO^+ core for odd values of n and having a VO_2^+ core for even values of n, which are surrounded by mostly electrostatically bound dioxygen molecules in their respective ground states. Despite these seemingly simple characteristics of the V^+/O_2 reactions, the kinetic schemes required for the detailed analysis are in part rather complex.

In the presence of water, exchange of the loosely bounded dioxygen ligands toward H_2O as well as consecutive ion hydration leading to larger clusters is observed. Whereas ligand exchange and association seems not to be hindered for $[V,O_5]^+$ and $[V,O_7]^+$, and probably even $[V,O_3]^+$, the VO^+ cation reacts quite inefficiently with water. Interestingly, even the degenerate $^{16}O/^{18}O$ exchange between VO^+ and water is very inefficient. The computational predictions provide a very helpful tool for the interpretation of the experimental findings. In particular, theory shows that the interconversion between the hydrated oxide ion $OV(OH_2)^+$ and the tautomeric dihydroxide $V(OH)_2^+$ is almost impossible in strictly bimolecular collisions of VO^+ and H_2O. However, the data also corroborate the suspicion that water may actively participate in tautomerization reactions in the gas phase.

Acknowledgment. The Berlin group appreciates financial support by the Deutsche Forschungsgemeinschaft (SFB 546), the Volkswagen-Stiftung, and the Fonds der Chemischen Industrie. Further, we thank the Konrad-Zuse Zentrum Berlin for generous allocation of computer time. The York group recognizes the continued support by the Natural Sciences and Engineering Research Council of Canada. The authors appreciate helpful comments by and cooperation with A. Irigoras Balda and J. Ugalde.

References and Notes

(1) *Appl. Catal. A*, **1997**, *157* (entire volume deals with this topic).

(2) (a) Almond, M. J.; Atkins, R. W. *J. Chem. Soc., Dalton Trans.* **1994**, 835. (b) Chertihin, G. V.; Bare, W. D.; Andrews, L. *J. Phys. Chem. A* **1997**, *101*, 5090.

(3) Wu, H.; Wang, L.-S. *J. Chem. Phys.* **1998**, *108*, 5310.

(4) For leading references, see: (a) Cundari, T. R.; Sisterhen, L. L.; Stylianopoulos, C. *Inorg. Chem.* **1997**, *36*, 4029. (b) Hamstra, B. J.; Colpas, G. J.; Pecoraro, V. L. *Inorg. Chem.* **1998**, *37*, 949.

(5) Eller, K.; Schwarz, H. *Int. J. Mass Spectrom. Ion Processes* **1989**, *93*, 243.

(6) Eller, K.; Zummack, W.; Schwarz, H. *J. Am. Chem. Soc.* **1990**, *112*, 621.

(7) Schröder, D.; Schwarz, H.; Clemmer, D. E.; Chen, Y.-M.; Armentrout, P. B.; Baranov, V. I.; Böhme, D. K. *Int. J. Mass Spectrom. Ion Processes* **1997**, *161*, 177.

(8) Mackay, G. I.; Vlachos, G. D.; Bohme, D. K.; Schiff, H. I. *Int. J. Mass Spectrom. Ion Phys.* **1980**, *36*, 259.

(9) Koyanagi, G. K.; Lavrov, V. V.; Baranov, V.; Bandura, D.; Tanner, S.; McLaren, J. W.; Bohme, D. K. *Int. J. Mass Spectrom.* **2000**, *194*, L1.

(10) Rue, C.; Armentrout, P. B.; Kretzschmar, I.; Schröder, D.; Harvey, J. N.; Schwarz, H. *J. Chem. Phys.* **1999**, *110*, 7858.

(11) Moore, C. E. *Atomic Energy Levels*, National Standard, Reference Data Series, National Bureau of Standards, NSRDS−NBS 35, Washington, DC, 1971.

(12) (a) Lee, C.; Yang, W.; Parr, R. G. *Phys. Rev B* **1988**, *37*, 785. (b) Miehlich, B.; Savin, A.; Stoll, H.; Preuss, H. *Chem. Phys. Lett.* **1989**, *157*, 200. (c) Becke, A. D. *J. Chem. Phys.* **1993**, *98*, 5648.

(13) *Gaussian 94* (Revision A.1), Frisch, M. J.; Trucks, G. W.; Schlegel, H. B.; Gill, P. M. W.; Johnson, B. G.; Robb, M. A.; Cheeseman, J. R.; Keith, T. A.; Petersson, G. A.; Montgomery, J. A.; Raghavachari, K.; Al-Laham, M. A.; Zakrzewski, V. G.; Ortiz, J. V.; Foresman, J. B.; Cioslowski, J.; Stefanov, B. B.; Nanayakkara, A.; Challacombe, M.; Peng, C. Y.; Ayala, P. Y.; Chen, W.; Wong, M. W.; Andres, J. L.; Replogle, E. S.; Gomperts, R.; Martin, R. L.; Fox, D. J.; Binkley, J. S.; Defrees, D. J.; Baker, J.; Stewart, J. P.; Head-Gordon, M.; Gonzalez, C.; Pople, J. A., Gaussian Inc., Pittsburgh 1995.

(14) Schafer, A.; Huber, C.; Ahlrichs, R. *J. Chem. Phys.* **1994**, *100*, 5829.

(15) Schafer, A.; Horn, H.; Ahlrichs, R. *J. Chem. Phys.* **1992**, *97*, 2571.

(16) (a) Irigoras, A.; Fowler, J. E.; Ugalde, J. M. *J. Am. Chem. Soc.* **1999**, *121*, 574. (b) Irigoras Balda, A. *Water dehydrogenation by first-row transition metal cations. A Paradigm for two-state reactivity*, Ph.D. Thesis, Andoain, Servicio Editorial de la Universidad del Pais Vasco, Spain, 1999.

(17) Throughout the paper, gas kinetic collision rates are calculated using the capture theory, see: Su, T. *J. Chem. Phys.* **1988**, *89*, 5355, and references therein.

(18) (a) Kappes, M. M.; Staley, R. H. *J. Chem. Phys.* **1981**, *85*, 942. (b) See also: Jackson, T. C.; Carlin, T. J.; Freiser, B. S. *J. Am. Chem. Soc.* **1986**, *108*, 1120.

(19) Kappes, M. M.; Staley, R. H. *J. Am. Chem. Soc.* **1981**, *103*, 1286.

(20) Plane, J. M. C.; Rollason, R. J. *J. Chem. Soc., Faraday Trans.* **1996**, *92*, 4371.

(21) Fisher, E. R.; Elkind, J. L.; Clemmer, D. E.; Georgiadis, R.; Loh, S. K.; Aristov, N.; Sunderlin, L. S.; Armentrout, P. B. *J. Chem. Phys.* **1990**, *93*, 2676.

(22) See also: Clemmer D. E.; Chen, T.-M.; Aristov, N.; Armentrout, P. B. *J. Chem. Phys.* **1999**, *110*, 7858.

(23) In the case of incomplete thermalization of the V^+ precursor, trace amounts of VOH^+ are also observed. Generation of VOH^+ from V^+/H_2O is clearly an endothermic process, which we attribute to the presence of some electronically excited V^+ under these circumstances.

(24) For a recent guide to the literature, see: Gapeev, A.; Dunbar, R. C. *J. Phys. Chem. A* **2000**, *104*, 4084, and references therein.

(25) See also: Kretzschmar, I.; Schröder, D.; Schwarz, H.; Rue, C.; Armentrout, P. B. *J. Phys. Chem. A* **1998**, *102*, 10060.

(26) (a) Brönstrup, M.; Schröder, D.; Schwarz, H. *Chem. Eur. J.* **1999**, *5*, 1176. (b) Bärsch, S.; Schröder, H.; Schwarz, H. *Chem. Eur. J.* **2000**, *6*, 1789.

(27) Blum, O.; Stöckigt, D.; Schröder, D.; Schwarz, H. *Angew. Chem.* **1992**, *104*, 637; *Angew. Chem., Int. Ed. Engl.* **1992**, *31*, 603.

(28) Jackson, P.; Harvey, J. N.; Schröder, D.; Schwarz, H. *Int. J. Mass Spectrom.* **2001**, *204*, 233.

(29) For a dramatic failure of DFT methods in describing $[Pt,O_2]^+$, see: Brönstrup, M.; Schröder, D.; Kretzschmar, I.; Schwarz, H.; Harvey, J. N. *J. Am. Chem. Soc.* **2001**, *123*, 142.

(30) The measured rate constant for $^{16}O/^{18}O$ exchange of $^{18}OV^{16}O^+$ with water is 1×10^{-10} cm^3 molecule^{-1} s^{-1}.

(31) Survey: Schröder, D.; Shaik, S.; Schwarz, H. In Metal-Oxo and Metal-Peroxo Species in Catalytic Oxidations in the series *Structure and Bonding*, Vol. 97; Meunier, B., Ed.; Springer, Berlin, 2000, p 91.

(32) (a) Sülzle, D.; Schwarz, H.; Moock, K. H.; Terlouw, J. K. *Int. J. Mass Spectrom. Ion Processes* **1991**, *108*, 269. (b) Schröder, D.; Fiedler, A.; Schwarz, J.; Schwarz, H. *Inorg. Chem.* **1994**, *33*, 5094. (c) Fiedler, A.; Kretzschmar, I.; Schröder, D.; Schwarz, H. *J. Am. Chem. Soc.* **1996**, *118*, 9941.

(33) Harvey, J. N.; Diefenbach, M.; Schröder, D.; Schwarz, H. *Int. J. Mass Spectrom. Ion Processes* **1999**, *182/183*, 85.

(34) Bärsch, S.; Schröder, D.; Schwarz, H. *Helv. Chim. Acta* **2000**, *83*, 827.

(35) Herzberg, G. *Molecular Spectra and Molecular Structure*, reprint edition; Krieger, Malabar; Vol. I, 1989 Vol III, 1991.

(36) Lide, D. R. *CRC Handbook Chemistry and Physics*, CRC Press: Boca Raton, 1998/99.

(37) Harrington, J.; Weisshaar, J. C. *J. Chem. Phys.* **1992**, *97*, 2809.

(38) Koch, W.; Holthausen, M. C. *A chemist's guide to density functional theory*; Wiley-VCH: Weinheim, 2000.

(39) Although $^1VO_2^+$ corresponds to a formal closed-shell singlet, as do most other transition metal dioxides, the molecule is bent. For an explanation of bending, see: Siegbahn, P. E. M. *J. Phys. Chem.* **1993**, *97*, 9096.

(40) All structures have been optimized in C_1 symmetry first, allowing the systems to adopt the most favorable geometries. Upon convergence to higher symmetries, the species have been further optimized in those symmetries. Several starting geometries have been investigated, which converged to one of the three geometries shown.

(41) Shriver, D. F.; Atkins, P. W.; Langford, C. H. *Inorganic Chemistry*, 2nd ed.; Freeman & Co.: New York, 1994.

(42) Ricca, A.; Bauschlicher, C. W., Jr. *J. Phys. Chem.* **1997**, *101*, 8949.

(43) Bohme, D. K. *Int. J. Mass Spectrom. Ion Processes* **1992**, *185*, 95.

(44) For a recent example using a slightly more complex rate expression in association kinetics, see: Schröder, D.; Brown, R.; Schwerdtfeger, P.; Schwarz, H. *Int. J. Mass Spectrom.* **2000**, *203*, 155.